

Inverse Compton Cascades in Pair-Producing Gaps:
Effects of Triplet Pair Production

MARIA PETROPOULOU,¹ YAJIE YUAN,¹ ALEXANDER Y. CHEN,¹ AND APOSTOLOS MASTICHIADIS²

¹*Department of Astrophysical Sciences, Princeton University
4 Ivy Lane, Princeton, NJ 08544, USA*

²*Department of Physics, National & Kapodistrian University of Athens
Panepistimiopolis, 15784 Zografos Greece*

(Received January 1, 2018; Revised January 7, 2018; Accepted August 6, 2019)

Submitted to ApJ

ABSTRACT

Inverse Compton-pair cascades are initiated when gamma-rays are absorbed on an ambient soft photon field to produce relativistic pairs, which in turn up-scatter the same soft photons to produce more gamma-rays. If the Compton scatterings take place in the deep Klein-Nishina regime, then triplet pair production ($e\gamma_b \rightarrow ee^+e^-$) becomes relevant and may even regulate the development of the cascade. We investigate the properties of pair-Compton cascades with triplet pair production in accelerating gaps, i.e., regions with an unscreened electric field. Using the method of transport equations for the particle evolution, we compute the growth rate of the pair cascade as a function of the accelerating electric field in the presence of black-body and power-law ambient photon fields. Informed by the numerical results, we derive simple analytical expressions for the peak growth rate and the corresponding electric field. We show that for certain parameters, which can be realized in the vicinity of accreting supermassive black holes at the centers of active galactic nuclei, the pair cascade may well be regulated by inverse Compton scattering in the deep Klein-Nishina regime and triplet pair production. We present indicative examples of the escaping gamma-ray radiation from the gap, and discuss our results in application to the TeV observations of radio galaxy M87.

Keywords: acceleration of particle – gamma-rays: galaxies – galaxies: active, individual (M87) – radiation mechanisms: non-thermal

1. INTRODUCTION

The production of a relativistic electron-positron pair from the absorption of a gamma-ray photon is the starting point of an avalanche of pairs and gamma rays, known as an electromagnetic (EM) cascade. Inverse Compton-pair cascades, in particular, are initiated when gamma-rays are absorbed on a soft photon field to produce relativistic pairs, which in turn inverse Com-

pton scatter off the same soft photons to produce more gamma-rays.

In the simplest case, where the pairs are not accelerated, only a few generations of them are expected to be produced before the energy of gamma-rays is degraded to a value below the threshold for $\gamma\gamma$ pair creation, thus ceasing the EM cascade. At this point, gamma-rays can escape unimpeded from the region of their production, with their initial energy being shared among the secondary pairs and photons. As long as the energy density of the secondary photons is lower than that of the background soft photon field, the cascade is considered to be *linear*, i.e., the interactions between secondary pairs and photons are negligible.

Corresponding author: Maria Petropoulou
m.petropoulou@astro.princeton.edu

Corresponding author: Yajie Yuan
yajiey@astro.princeton.edu

Linear inverse Compton-pair cascades in isotropic photon fields¹ have been discussed in the context of compact X-ray sources (Akharonian et al. 1985; Mastichiadis 1986; Zdziarski et al. 2009) and applied to the propagation of ultra-high-energy (UHE) gamma-rays in the intergalactic medium (IGM) (Gould & Rephaeli 1978; Protheroe 1986; Zdziarski 1988; Coppi & Aharonian 1997). In the latter case, the initial Compton scatterings of UHE pairs on low-energy background photons (e.g., cosmic microwave background) can take place deep in the Klein-Nishina regime (i.e., $s \gg (m_e c^2)^2$, where s is the squared center-of-mass energy of the interaction). In this regime, triplet pair production (TPP; $e\gamma_b \rightarrow ee^+e^-$) can be an additional source of electron cooling. Although TPP is a third-order quantum electrodynamical process, it can operate in direct competition to inverse Compton scattering (ICS) for $s \gtrsim 100 \text{ MeV}^2$ (Haug 1981; Mastichiadis et al. 1986; Mastichiadis 1991; Anguelov et al. 1999). Because of the very high interaction energies required, the role of TPP has been mainly investigated in the context of UHE-photon induced cascades in the IGM (Lee 1998; Settimo & De Domenico 2015; Wang et al. 2017).

The vicinity of supermassive black holes in active galactic nuclei (AGN), where strong electric fields may be present and copious soft photons are emitted by the accretion disk, is another astrophysical environment where linear Compton-pair cascades have been studied (e.g., Bednarek & Kirk 1995; Levinson & Rieger 2011; Broderick & Tchekhovskoy 2015; Hirovani & Pu 2016; Chen et al. 2018; Katsoulakos & Rieger 2018; Levinson & Cerutti 2018). In this case, the physics of the cascade are coupled to the acceleration of particles by the component of the electric field parallel to the magnetic field over the length of a charge-starved region, the so-called gap². A seed electron that enters the gap can accelerate to high enough energies to up-scatter disk photons and produce gamma-rays, which in turn pair-produce on the disk photons, thus initiating a pair cascade in the gap. In contrast to the cascades induced in the IGM, the secondary electrons are continuously accelerated inside the gap. This leads to an exponentiation of their number density until they provide the necessary charge density to sort out the electric field and quench acceleration.

¹ The development of these cascades in anisotropic photon fields was studied by Protheroe et al. (1992).

² There is an analogy to pair cascades in pulsar magnetospheres (Ruderman & Sutherland 1975), although the physical processes related to the production of gamma-ray photons are different (see e.g., Timokhin & Arons 2013; Timokhin & Harding 2019, and references therein).

In this paper, we study the generic properties of inverse Compton cascades in pair-producing gaps in the Thomson and Klein-Nishina regimes with the inclusion of triplet pair production. More specifically, we compute the growth rate of secondary pairs as a function of the electric field strength for a background soft photon field (with a black-body or power-law energy distribution) and study the effects of triplet pair production on the development of these cascades (e.g., growth rate and maximum particle energy). This paper is structured as follows. In Section 2 we qualitatively discuss the general properties of Compton-pair cascades with triplet pair production. In Section 3 we outline the adopted numerical scheme for the calculation of the cascade and present our results on the pair growth rate in Section 4. We discuss their astrophysical implications in Section 5 and conclude with a discussion on the model's caveats in Section 6.

2. GENERAL CONSIDERATIONS

We consider a stationary rectilinear particle accelerator immersed in an isotropic time-independent ambient photon field with energy density $U_{ph} \equiv \int d\epsilon \epsilon n_b(\epsilon)$, where $n_b(\epsilon)$ is the differential photon number density. The accelerator is characterized by a constant electric field with strength E_0 . The electric field is assumed to be almost parallel to the local magnetic field, which has no curvature. The size of the acceleration region is taken to be much larger than all relevant mean free paths of relativistic pairs, thus allowing us to follow the full development of the pair cascade.

Within our toy model, we treat electrons and positrons as identical particles with initial Lorentz factor γ_0 . Upon entering the acceleration region, pairs will gain energy from the electric field, and at the same time, lose energy due to ICS (or TPP) on the background soft photon field. Energy losses due to synchrotron and curvature radiation can be neglected under our assumptions (i.e., the particle pitch angle and the curvature of magnetic field lines are both approximately zero).

As long as the scatterings occur in the Thomson regime, particles can accelerate from their initial Lorentz factor to a maximum value γ_{eq} where the continuous energy losses balance the energy gains:

$$\gamma_{eq} = \left(\frac{3q_e E_0}{4\sigma_T U_{ph}} \right)^{1/2}. \quad (1)$$

In the above equation c is the speed of light, σ_T is the Thomson cross section, and q_e, m_e are the electron charge and mass. The scattering of soft photons with energy $\langle \epsilon \rangle \equiv \int d\epsilon \epsilon n_b(\epsilon) / \int d\epsilon n_b(\epsilon)$ by pairs with Lorentz factor γ_{eq} will occur in the Klein-Nishina regime, if E_0

exceeds a critical value that depends solely on the properties of the target photon field, namely:

$$E_0^{(\text{KN})} = \frac{4\sigma_T U_{ph}}{3q_e} \left(\frac{m_e c^2}{\langle \epsilon \rangle} \right)^2, \quad (2)$$

where we used the condition $\gamma_{eq} \langle \epsilon \rangle \gtrsim (3/4)m_e c^2$ and Equation (1). In particular, for a black-body photon field with temperature T we find $E_0^{(\text{KN})} \propto T^2$. Using this critical value of the electric field, we can distinguish the following two regimes.

Low- E_0 regime: for $E_0 < E_0^{(\text{KN})}$ the acceleration process is balanced by energy losses mostly in the Thomson regime and the particle Lorentz factor saturates at the value given by Equation (1). As a result, the up-scattered photons, of energy $\epsilon_1 \sim \gamma_{eq}^2 \langle \epsilon \rangle$, are below the threshold for $\gamma\gamma$ production with the average energy soft photons (i.e., $\epsilon_1 \langle \epsilon \rangle < 2(m_e c^2)^2$). Still, pair production is expected to occur at some level due to $\gamma\gamma$ interactions with photons from the high-energy tail of the distribution. We note that TPP is not relevant in this regime due to the much lower interaction rates (see e.g., Fig. 4 in Mastichiadis 1991). The number density of photons at $\epsilon \gg \langle \epsilon \rangle$ together with the rate of acceleration will essentially determine the growth rate of the produced pairs. For a black-body photon field, there is essentially no free parameter other than E_0 , since the photon number density at $\epsilon \gg \langle \epsilon \rangle \simeq 2.7k_B T$ is just given by the Wien part of the spectrum. However, in the more general case of a power-law photon field, the exact growth rate of the number of pairs is expected to depend on several free parameters: the maximum and minimum cutoff energies ($\epsilon_{\text{max}}, \epsilon_{\text{min}}$), the photon index (Γ), and the energy density (U_{ph}).

High- E_0 regime: for $E_0 > E_0^{(\text{KN})}$, pairs can achieve much higher Lorentz factors than γ_{eq} (see Equation (1)); the highest energy pairs can up-scatter soft photons in the Klein-Nishina regime, where the energy losses are not strong enough to balance the energy gains by the acceleration. As a result, the maximum particle energy does not saturate at γ_{eq} , but continues to increase till another process (e.g., physical escape from the system) settles in. Quickly upon entering the acceleration region, the seed pairs can achieve high enough energies to produce secondary pairs off the photon field either directly through TPP or indirectly through the combination of ICS and $\gamma\gamma$ absorption. In both cases, the produced pairs will also be accelerated by the strong electric field, and their number will exponentiate.

In both regimes, a pair cascade will develop in the acceleration region. The cascade is, in good approximation, one-dimensional as long as the magnetic deviations of the particle trajectories over the relevant particle in-

teraction lengths are smaller than the emission cone of the pairs. Our goal is to compute the growth rate of the ensued linear pair cascade as a function of E_0 for different ambient photon fields. In the following section, we describe the numerical approach we adopted for the study of the pair cascade.

3. NUMERICAL APPROACH

The physical problem outlined in Section 2 can be mathematically formulated using the concept of transport equations that describe the evolution of three particle populations, namely the seed pairs that enter the acceleration region, the secondary pairs produced by $\gamma\gamma$ and TPP processes, and the photons emitted by both pair populations via ICS:

$$\frac{\partial n_e^{(1)}}{\partial t} + q_e c E_0 \frac{\partial n_e^{(1)}}{\partial \gamma} + \mathcal{L}_e^{ics} + \mathcal{L}_e^{tpp} = \mathcal{Q}_e^{inj} \quad (3)$$

$$\frac{\partial n_e^{(2)}}{\partial t} + q_e c E_0 \frac{\partial n_e^{(2)}}{\partial \gamma} + \mathcal{L}_e^{ics} = \mathcal{Q}_e^{tpp} + \mathcal{Q}_e^{\gamma\gamma} \quad (4)$$

$$\frac{\partial n_\gamma}{\partial t} + \mathcal{L}_\gamma^{\gamma\gamma} = \mathcal{Q}_\gamma^{ics}. \quad (5)$$

Here, $n_e^{(1)}$, $n_e^{(2)}$, and n_γ denote respectively the differential number densities of seed pairs, secondary pairs, and photons produced by both populations of pairs. The operators \mathcal{Q}_i^j and \mathcal{L}_i^j denote injection and loss terms of the particle species i due to the process j .

To solve the particle transport equations, we employ the numerical code of Mastichiadis & Kirk (1995), but with two main modifications: the implementation of the triplet pair production process and the use of a more accurate scheme for the treatment of electron losses in the Klein-Nishina regime. For completeness, we summarize the different terms appearing in eqs. (3)-(5) briefly.

Pair injection. Seed pairs with some low Lorentz factor are injected into the acceleration region at a rate $\mathcal{Q}_e^{inj} = Q_0 \delta(\gamma - \gamma_0) H(t)$. Here, we adopted (without loss of generality) $\gamma_0 = 1$. We checked that the derived exponential growth rates (see Section 4) do not depend on the choice of γ_0 or of the injection profile (e.g., continuous versus instantaneous injection).

Inverse Compton scattering. The term \mathcal{L}_e^{ics} takes into account energy losses in both the Thomson and Klein-Nishina regimes according to Eqs. (5.7) and (5.17) of Blumenthal & Gould (1970). For the photon production rate \mathcal{Q}_γ^{ics} we use Eq. (2.48) of Blumenthal & Gould (1970).

$\gamma\gamma$ pair production. The pair injection term $\mathcal{Q}_e^{\gamma\gamma}$ and photon attenuation rate $\mathcal{L}_\gamma^{\gamma\gamma}$ are given respectively by Eqs. (57) and (54) of Mastichiadis & Kirk (1995).

Triplet pair production. We consider the energy losses of the recoiling electron (or positron)

to be continuous. For the single-particle loss rate q_{tpp} we adopt the Eq. (29) of Mastichiadis (1991), which holds away from the interaction threshold ($\gamma\epsilon > 10^3 m_e c^2$). The exact functional form of q_{tpp} near the threshold is not important, since ICS losses dominate in this energy regime (Mastichiadis 1991). The loss term appearing in Equation (3) is modeled as $\mathcal{L}_e^{tpp}(\gamma) = \int d\epsilon n_b(\epsilon) q_{tpp}(\gamma\epsilon/m_e c^2)$. Following Lee (1998), we model the TPP production rate as $\mathcal{Q}_e^{tpp}(\gamma') = q_0 \gamma'^{-\delta} \int d\gamma n_e^{(1)}(\gamma) \int d\epsilon \sigma_{tpp}(\gamma\epsilon/m_e c^2) n_b(\epsilon)$, where σ_{tpp} is the total TPP cross section (Haug 1981; Mastichiadis 1991). We adopt the asymptotic value of 7/4 for the exponent δ (see also Fig. 2 in Mastichiadis 1991), while noting that our results are not sensitive on the exact value of δ . The normalization constant q_0 is determined by the requirement of energy conservation, i.e., $\int d\gamma n_e^{(2)}(\gamma) \gamma \mathcal{Q}_e^{tpp}(\gamma) = \int d\gamma n_e^{(1)}(\gamma) \gamma \mathcal{L}_e^{tpp}(\gamma)$.

Finally, we note that the numerical code solves for the combined distribution $n_e = n_e^{(1)} + n_e^{(2)}$. Although the code does not differentiate between seed pairs and secondary pairs, any exponentially growing solutions of n_e are purely determined by the secondaries. This can be easily understood by considering the extreme case of no pair production ($n_e^{(2)} = 0$). In this case, one can show by solving Equation (3) with $\mathcal{L}_e^{tpp} = 0$ that the lepton number $\int n_e(\gamma) d\gamma$ increases only linearly with time.

4. RESULTS

Using the numerical code described in the previous section, we compute the growth rate (λ) of exponentially increasing solutions for a wide range of electric field strengths E_0 and different ambient photon fields. More specifically, we perform a linear fit to $y(t) \equiv \ln[\int d\gamma n_e(\gamma, t)]$, since its slope gives directly the rate of exponentially growing solutions. In what follows, we compute λ for a black-body photon field of temperature T (Section 4.1) and for a power-law photon field with photon index Γ and energy density U_{ph} , extending from ϵ_{min} to ϵ_{max} (Section 4.2).

4.1. Black-body photons

Figure 1 presents the exponential growth rate λ computed numerically for different electric field strengths E_0 when: (i) both $\gamma\gamma$ and triplet pair production processes are taken into account (filled symbols), (ii) only triplet pair production is taken into account (open triangles), and (iii) only $\gamma\gamma$ pair production is included (open circles). Note that the growth rate in the absence of pair production asymptotes to a constant value instead of approaching zero (see e.g., filled symbols at $E_0 \lesssim 10^{-2}$ statV cm $^{-1}$ and open circles at $E_0 > 10^3$ statV cm $^{-1}$). This is a result of our choice for the injection of

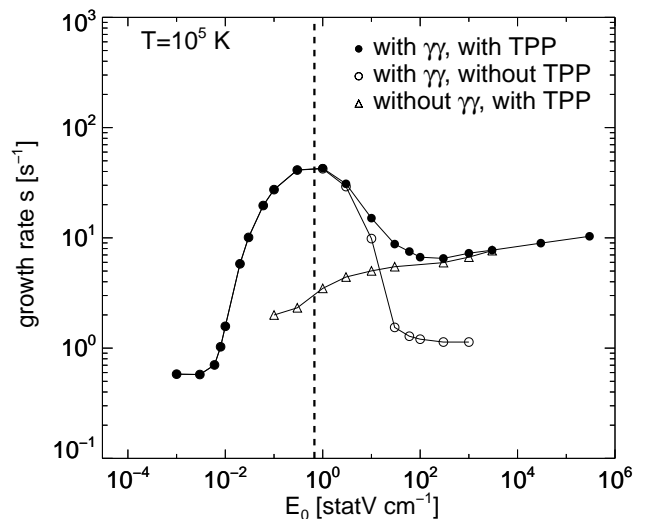


Figure 1. Growth rate of the number of pairs as a function of the electric field strength E_0 , for a black-body photon field with temperature $T = 10^5$ K. Different symbols are used to plot the growth rates when different processes are taken into account (for details, see inset legend). The vertical dotted line indicates the critical value of the electric field given by Equation (2).

seed particles (see also Section 3). With a continuous injection, even in the absence of any pair production processes ($n_e^{(2)} = 0$), the number of seeds is expected to increase linearly with time. These non-exponential growing solutions are reflected to the non-zero values of the numerically derived growth rates³.

The actual shape of the curve $\lambda(E_0)$ is determined by the convolution of the ambient photon field energy distribution with the energy-dependent cross sections of the relevant physical processes. In the low- E_0 regime (i.e., for $E_0 < E_0^{(KN)}$), the growth rate is determined essentially by the $\gamma\gamma$ pair production process. However, in the high- E_0 regime ($E_0 > E_0^{(KN)}$), where the $\gamma\gamma$ cross section decreases (see open circles), triplet pair production begins to take over and eventually dominates the total growth rate of pairs at $\gtrsim 100 E_0^{(KN)}$ (open triangles). In this regime, the slow increase of λ with increasing E_0 reflects the logarithmic dependence of the TPP cross section (see also Figure 3 and text in Section 4.2, for more details).

³ We verified that $\lambda \rightarrow 0$ for sufficiently low or high (in the absence of TPP) electric field strengths, if seed particles are instantaneously injected into the gap

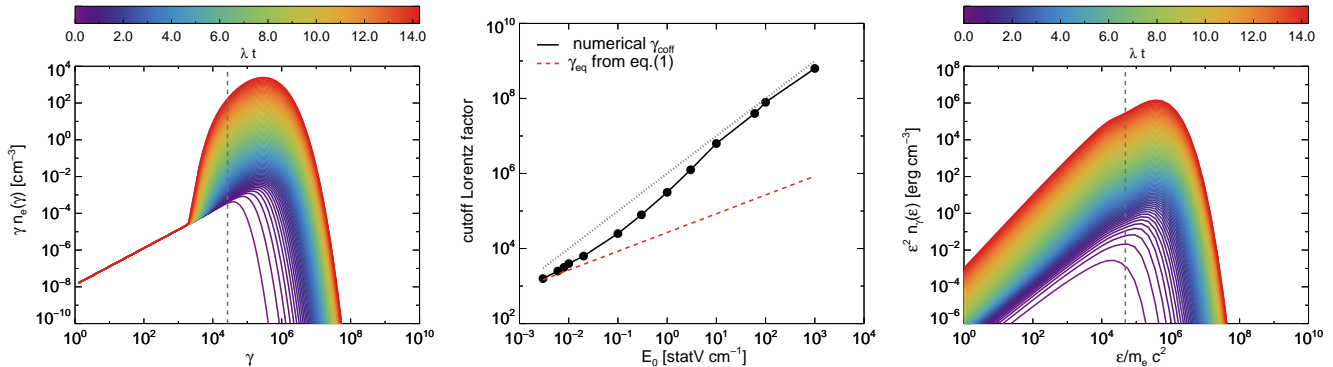


Figure 2. *Left panel:* Temporal evolution of the pair energy distribution (colored lines) for the same photon field used in Fig. 1 and $E_0 = 1 \text{ statV cm}^{-1} \simeq E_0^{(\text{KN})}$. Here, both $\gamma\gamma$ and triplet pair production processes are taken into account. The color bar indicates the time (in units of the growth time λ^{-1}). The dashed vertical line marks the saturation Lorentz factor for IC losses in the Thomson regime given by Equation (1). *Middle panel:* Cutoff Lorentz factor of the pair energy distribution computed numerically for different electric field strengths (black symbols). The dashed red line shows γ_{eq} defined in Equation (1). A line of slope one (dotted grey) is overplotted to illustrate the asymptotic scaling of the cutoff Lorentz factor on E_0 , when TPP dominates. *Right panel:* Snapshots of the IC photon energy spectrum (colored lines) produced in the gap. The dashed vertical line marks the typical up-scattered photon energy of $4k_B T \gamma_{\text{eq}}^2$. The color bar indicates the time (in units of the growth time λ^{-1}) or, equivalently, the location within the gap at which the spectrum is produced. The last snapshot shown here should be considered as the escaping photon spectrum from a gap with size $h = 14c/\lambda \simeq 10^{10}$ cm.

As an indicative example, we show in Figure 2 (left panel) the temporal evolution of the pair energy distribution computed for $E_0 = 1 \text{ statV cm}^{-1} \simeq E_0^{(\text{KN})}$, when both pair production processes are taken into account. The dashed vertical line marks the saturation Lorentz factor assuming ICS losses in the Thomson regime (see Equation (1)). The energy spectrum can be modeled as $\gamma n_e(\gamma) \propto \gamma e^{-\gamma/\gamma_{\text{coff}}}$, where γ_{coff} is generally time-dependent. Before the number of pairs exponentiates (i.e., $t \lesssim \lambda^{-1}$), we find that $\gamma_{\text{coff}} \propto t$ and $\gamma_{\text{coff}} \gtrsim \gamma_{\text{eq}}$. The extension of the spectrum beyond γ_{eq} suggests that the up-scattering of black-body photons with energy $\langle \epsilon \rangle = 2.7k_B T$ by pairs with $\gamma \gtrsim \gamma_{\text{eq}}$ takes place in the Klein-Nishina regime, already from $E_0 \sim E_0^{(\text{KN})}$.

Soon after the onset of the cascade (i.e., $t \gtrsim \lambda^{-1}$), the cutoff Lorentz factor of the distribution freezes at a value that depends on E_0 . This is illustrated in the middle panel of Figure 2, where we plot the time-independent γ_{coff} determined numerically for different electric field strengths. The dashed red line denotes the saturation Lorentz factor considering particle losses only in the Thomson regime (see Equation (1)). As soon as pair production becomes important, we find that $\gamma_{\text{coff}} > \gamma_{\text{eq}}$. For the adopted parameters, this occurs at $E_0 \gtrsim 10^{-2} \text{ statV cm}^{-1}$ (see also Fig. 1). In the high- E_0 regime, in particular, the dependence of γ_{coff} on E_0 can be derived from the following condition: any pairs injected via the TPP process should reach the Lorentz factor γ of the parent electron within the mean

free path of the process, namely $m_e \gamma c^2 \approx eE_0 \ell_{\text{tpp}}(\gamma)$ with $\ell_{\text{tpp}}^{-1}(\gamma) \approx \int d\epsilon n_b(\epsilon) \sigma_{\text{tpp}}(\gamma\epsilon/m_e c^2)$. For a black-body photon distribution, we find $\ell_{\text{tpp}}(\gamma) \approx \text{constant}$ and $\gamma_{\text{coff}}^{(\text{tpp})} \propto E_0$, in agreement with the numerical results for $E_0 \gtrsim 30 \text{ statV cm}^{-1}$, where the pair production is regulated via the TPP process (see also Figure 1).

The right panel of Figure 2 shows snapshots of the photon energy spectra produced by ICS off an ambient black-body photon field by the pairs in the accelerating gap (see left panel of the same figure). For reference, the typical photon energy of $4\gamma_{\text{eq}}^2 k_B T$ is also indicated (dashed grey line). Each snapshot corresponds to a certain time (in units of λ^{-1}) or, equivalently, a certain location within the gap. If the physical size of the latter is taken to be $h = 14c/\lambda = 10^{10}$ cm, then the last snapshot shown in the figure would correspond to the spectrum of photons escaping from the gap. Note that this would not necessarily be the observed spectrum, because other processes operating outside the gap could still alter it (for further discussion, see Section 5.1).

4.2. Power-law photons

Figure 3 presents the exponential growth rate λ as a function of E_0 for an ambient photon field with a power-law energy distribution. Here, both $\gamma\gamma$ and triplet pair production are considered. Different panels (from left to right) demonstrate the effects of U_{ph} , ϵ_{min} , and Γ on the growth rate (for details, see figure caption and inset legends). By varying the photon energy density, while keeping all other parameters fixed (left panel), we obtain

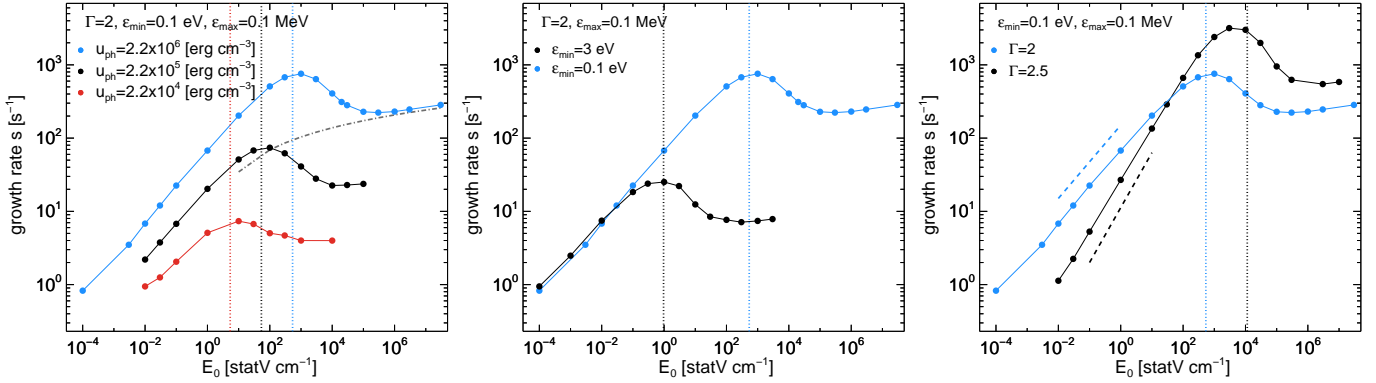


Figure 3. Same as in Fig. 1, but for a power-law target photon field with $\Gamma = 2$, $\epsilon_{\min} = 0.1$ eV, $\epsilon_{\max} = 0.1$ MeV, and $U_{ph} = 2.2 \times 10^6$ erg cm $^{-3}$, unless stated otherwise. We show the dependence of the growth rate (from left to right) on the photon energy density, minimum photon energy, and photon index. In all panels, vertical dotted lines mark the critical value of E_0 given by Equation (2). The dashed lines plotted in the right panel have slopes $(\Gamma - 1)/2$, as analytically predicted (see Equation (11)). We also predict $\lambda \propto \ln E_0$ for $E_0 \gg E_0^{(\text{KN})}$ (see Equation (12)), as shown in the left panel (dash-dotted grey line). A colored version of this plot is available online.

a self-similar family of curves for $\lambda(E_0)$. For example, if we were to shift the black curve to the right and upwards by a factor of 10 in each direction, we would obtain the blue curve. More specifically, the peak growth rate λ_{\max} and the electric field strength at the peak scale linearly with U_{ph} . The latter scaling agrees with the predicted one for $E_0^{(\text{KN})}$ (see Equation (2)).

The growth rate depends also on ϵ_{\min} , as shown in the middle panel, for fixed U_{ph} and Γ . In particular, we find larger growth rates for lower ϵ_{\min} , as the latter translates to a higher number density of low energy photons, acting as targets for ICS and pair production. Were the black curve shifted to the right by a factor of $\sim 30^2$ and upwards by a factor of ~ 30 , it would match the blue curve. Thus, for fixed U_{ph} and Γ we find $\lambda_{\max} \propto \epsilon_{\min}^{-1}$. This also translates to $\lambda_{\max} \propto \langle \epsilon \rangle^{-1}$, where the mean photon energy for a power-law photon field is:

$$\langle \epsilon \rangle = \begin{cases} \epsilon_{\min} \ln \left(\frac{\epsilon_{\max}}{\epsilon_{\min}} \right) \left(1 - \frac{\epsilon_{\min}}{\epsilon_{\max}} \right)^{-1}, & \Gamma = 2 \\ \frac{-\Gamma+1}{-\Gamma+2} \frac{\epsilon_{\max}^{-\Gamma+2} - \epsilon_{\min}^{-\Gamma+2}}{\epsilon_{\max}^{-\Gamma+1} - \epsilon_{\min}^{-\Gamma+1}}, & \Gamma \neq 2 \end{cases} \quad (6)$$

Finally, the effects of the photon index on the growth rate are presented in the right panel of Figure 3. We find that changes on Γ are imprinted on both the peak growth rate and the slope of the power-law segment of $\lambda(E_0)$ at $E_0 < E_0^{(\text{KN})}$. By changing the photon index and keeping all other parameters fixed, we are effectively varying the mean photon energy of the power-law distribution. This explains why the peak electric field $\approx E_0^{(\text{KN})}$ scales as $\langle \epsilon \rangle^{-2}$ (see Equation (2)). We also verified that the peak growth rates of the black and blue

curves match, if the black curve is shifted downwards by a factor equal to the ratio of the mean photon energies. Our numerical results also suggest that $\lambda \propto E_0^{(\Gamma-1)/2}$ in the low- E_0 regime. In what follows, we present analytical arguments to explain the power-law dependence of the growth rate on the photon index.

The growth rate is proportional to the number of generations of pairs produced per unit time. The latter, denoted as κ , can be estimated as $\kappa \approx c/(\ell_{\text{acc}} + \ell_{\text{IC}} + \ell_{\gamma\gamma})$, where ℓ_{acc} is the acceleration length, ℓ_{IC} is the IC scattering mean free path, and $\ell_{\gamma\gamma}$ is the $\gamma\gamma$ collision mean free path. When ICS is in Thomson regime, particles reach a terminal Lorentz factor as determined from Equation (1). As these particles IC scatter soft photons from different segments of the power-law energy spectrum, their mean free paths will also be different. Let $n_b(\epsilon) = n_0(\epsilon/\epsilon_{\min})^{-\Gamma}$ be the differential number density of the ambient photon field. Then, the mean free path for ICS on photons of energy ϵ is roughly:

$$\ell_{\text{IC}}(\epsilon) \approx \frac{1}{\sigma_T n_b(\epsilon) \epsilon} = \frac{\epsilon^{\Gamma-1}}{\sigma_T n_0 \epsilon_{\min}^{\Gamma}}. \quad (7)$$

The ICS on these soft photons produces high energy photons of energy $\epsilon_1 \approx \gamma_{\text{eq}}^2 \epsilon$, which can then interact with soft photons to produce pairs. The most likely target soft photons for $\gamma\gamma$ pair production are those near the threshold of the interaction, namely their energy is $\epsilon_t \approx (m_e c^2)^2 / \epsilon_1$, and the $\gamma\gamma$ mean free path is:

$$\ell_{\gamma\gamma}(\epsilon_t) \sim \frac{1}{\sigma_{\gamma\gamma} n_b(\epsilon_t) \epsilon_t} = \frac{\epsilon_t^{\Gamma-1}}{\sigma_{\gamma\gamma} n_0 \epsilon_{\min}^{\Gamma}}. \quad (8)$$

The peak cross section of the $\gamma\gamma$ pair production process (near the threshold) is similar to the Thomson cross section ($\sigma_{\gamma\gamma} \approx \sigma_T/5$, Gould & Schröder 1967). So, if the target photons for ICS have low ϵ , then $\ell_{\text{IC}}(\epsilon)$ is small, but $\ell_{\gamma\gamma}(\epsilon_t)$ of the most-likely-to-be attenuated photons is large, and *vice versa*. As a result, pair production is most efficient on target photons that have similar mean free paths for ICS and $\gamma\gamma$ pair production. This essentially means that $\epsilon \approx \epsilon_t \approx m_e c^2 / \gamma_{eq}$.

Moreover, in the low- E_0 regime, the acceleration length ℓ_{acc} is typically much smaller than the interaction mean free paths. The condition $\ell_{\text{acc}}(\gamma_{eq}) \lesssim \ell_{\text{IC}}(\epsilon = m_e c^2 / \gamma_{eq})$ can be written as:

$$\gamma_{eq} \epsilon_{\text{min}} \lesssim m_e c^2 \left(\frac{4/3}{\Gamma - 2} \right)^{1/(\Gamma - 2)}, \Gamma > 2 \quad (9)$$

$$\ln \left(\frac{\epsilon_{\text{max}}}{\epsilon_{\text{min}}} \right) \gtrsim 3/4, \Gamma = 2. \quad (10)$$

Noting that $\gamma_{eq} \epsilon_{\text{min}} < \gamma_{eq} \langle \epsilon \rangle < m_e c^2$, both conditions are easily satisfied in the low- E_0 regime. Thus, the generation rate of pairs can be estimated by:

$$\kappa \propto \frac{c}{\ell_{\text{IC}}(\epsilon = m_e c^2 / \gamma_{eq})} \propto \gamma_{eq}^{\Gamma - 1} \propto E_0^{\frac{\Gamma - 1}{2}}, \quad (11)$$

which roughly agrees with the slope we obtain from the numerical calculations (see right panel in Figure 3).

In the high- E_0 regime, and in particular at $E_0 \gg E_0^{(\text{KN})}$, pairs are injected into the acceleration region via the TPP process. The mean free path of a high-energy electron with Lorentz factor $\gamma < 2m_e c^2 / \epsilon_{\text{min}}$ is $\propto \gamma^{-\Gamma + 1}$, while it has only a logarithmic dependence on γ otherwise, i.e., $\ell_{\text{tpp}}(\gamma) \propto \ln^{-1}(2\gamma \epsilon_{\text{min}} / m_e c^2)$. The latter case is typically satisfied in the high- E_0 regime, where pairs are ultra-relativistic and their acceleration length is not anymore negligible. Pair production is most efficient when $\ell_{\text{acc}}(\gamma) \approx \ell_{\text{tpp}}(\gamma) \Rightarrow \gamma \propto E_0$, where the latter relation is derived after neglecting the logarithmic dependence of the TPP mean free path on the Lorentz factor. This condition also gives an estimate of the cutoff Lorentz factor of the pair distribution⁴, as discussed in Sec. 4.1 for a black-body photon field (see also Fig. 2). The number of pairs in the deep high- E_0 regime is therefore estimated as:

$$\kappa \propto \frac{c}{\ell_{\text{tpp}}(\gamma = \gamma_{\text{coff}}^{(\text{tpp})})} \propto \ln E_0, \quad (12)$$

⁴ When TPP is the dominant source of secondary pairs, the cutoff Lorentz factor of the pair distribution can be derived by $\ell_{\text{acc}}(\gamma_{\text{coff}}) \approx \ell_{\text{tpp}}(\gamma_{\text{coff}})$. Thus, $\gamma_{\text{coff}}^{(\text{tpp})} \propto E_0^{1/\Gamma} < 2m_e c^2 / \epsilon_{\text{min}}$ and $\gamma_{\text{coff}}^{(\text{tpp})} \propto E_0 > 2m_e c^2 / \epsilon_{\text{min}}$. Typically, only the latter branch is relevant, since at low Lorentz factors pair production is regulated by ICS and $\gamma\gamma$ processes.

which agrees with the logarithmic scaling of the growth rate determined numerically (see dash-dotted line in the left panel of Figure 3).

Based on the self-similarity of the numerical results shown in Figure 3 and the analytical arguments for the dependence of the growth rate on the photon index in the low- E_0 regime, we may write the following analytical expression for the growth rate:

$$\lambda \approx \lambda_{\text{max}} \left(\frac{E_0}{E_0^{(\text{KN})}} \right)^{\frac{\Gamma - 1}{2}}, \quad E \leq E_0^{(\text{KN})} \quad (13)$$

and its maximum value:

$$\lambda_{\text{max}} \approx 481 \frac{U_{ph,6}}{\langle \epsilon \rangle_0} [\text{s}^{-1}], \quad (14)$$

where $U_{ph} \equiv 10^6 U_{ph,6}$ erg cm⁻¹ and $\langle \epsilon \rangle \equiv 10^0 \langle \epsilon \rangle_0$ eV.

5. ASTROPHYSICAL APPLICATIONS

A funnel-like region forming at the interface of a jet with the accretion flow of a black hole (e.g., Bednarek & Kirk 1995) or a magnetospheric gap (e.g., Blandford & Znajek 1977; Beskin et al. 1992; Hirokani & Okamoto 1998) could be considered astrophysical analogues of our simplified particle accelerator.

In the case of a gap in the black-hole magnetosphere, it has been shown that the development of a non-ideal electric field and its screening can be highly time variable (Chen et al. 2018). Let us consider a flux tube threading the black hole horizon. At small distances within the tube particles fall into the black hole, while at large distances particles are flung outward by magnetocentrifugal effects. As a result, charge carriers get gradually depleted in the flux tube, leading to the growth of a non-ideal electric field when particles are not enough to carry the necessary current. Before any significant pair production happens, the electric field increases almost quadratically with time, so the time needed for the electric field to grow up to E_0 can be approximated as (Chen et al. 2018):

$$t_E \approx \frac{E_0}{\dot{E}} \approx \left(2\pi \frac{E_0}{B_0} \right)^{1/2} \frac{r_g}{c}, \quad (15)$$

where $r_g = 2GM_{\text{BH}}/c^2$ is the gravitational radius of a black hole with mass M_{BH} and B_0 is the strength of the poloidal magnetic field near the black-hole horizon. If the acceleration time of the particles is much shorter than the timescale for electric field growth, then the assumption of a constant electric field adopted here is valid (see Section 6 for a discussion on the validity of this assumption). A crude criterion for the screening of the gap

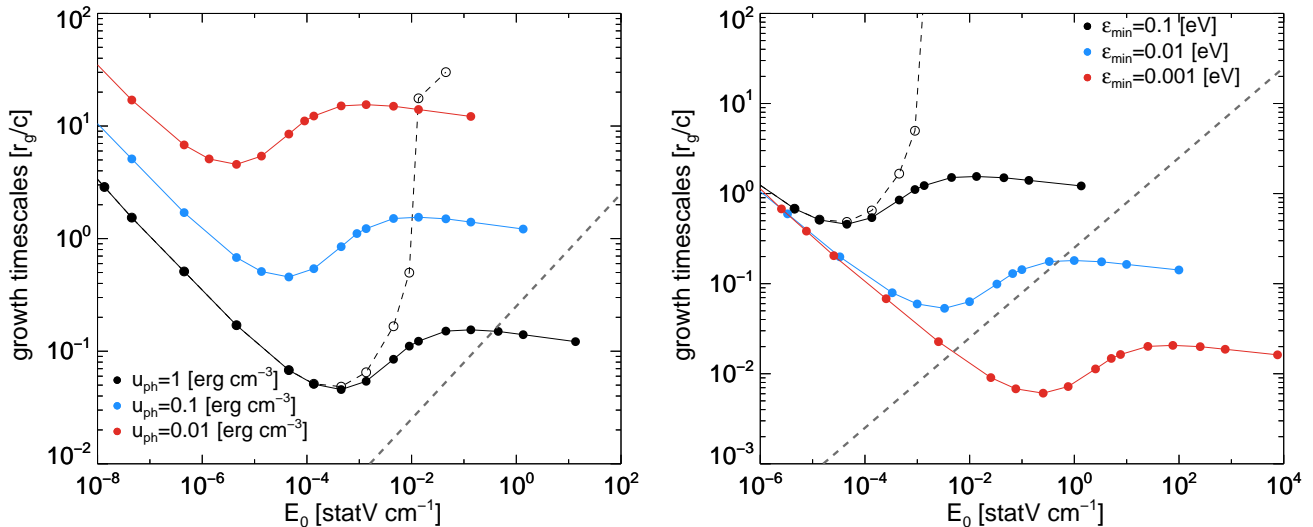


Figure 4. *Left panel:* Growth timescale of the number of pairs as a function of the electric field E_0 for power-law photon fields with $\Gamma = 2$, $\epsilon_{\min} = 0.1$ eV, $\epsilon_{\max} = 0.1$ MeV, and different energy densities marked on the plot. All curves are obtained by rescaling the numerical results shown in Figure 3 for $U_{ph} = 2.2 \times 10^6$ erg cm $^{-3}$ according to eqs. (2), (6), and (14). For one case, we also show for illustrative purposes the exponential growth time without TPP (open black symbols). *Right panel:* Same as in the left panel, but for different values of ϵ_{\min} marked on the plot. Here, $U_{ph} = 0.1$ erg cm $^{-3}$. In both panels, we plot a proxy for the electric field growth time given by Equation (15) for $B_0 = 10^2$ G (dashed grey line). All timescales are normalized to r_g/c , where $r_g \simeq 2 \times 10^{15}$ cm, which is also the gravitational radius of M87* (Event Horizon Telescope Collaboration et al. 2019). A colored version of this plot is available online.

is that the pair exponentiation timescale becomes comparable to or shorter than the timescale for the electric field growth given by Equation (15).

In Figure 4 we show the growth timescale of the Compton-pair cascade (colored curves) for a power-law background photon field with different energy densities and minimum energies (for details, see plot legends). The cascade timescale is large at small E_0 , but becomes smaller than t_E (dashed grey line) for sufficiently large E_0 . The equality of the two timescales gives an estimation of the maximum electric field that can develop in an electrostatic gap before it is screened, i.e., before the number density of pairs exceeds the Goldreich-Julian density $n_{GJ} = \Omega B_0 / 2\pi e c \approx \alpha B_0 / 4\pi e r_g \simeq 1.7 \times 10^{-5} B_{0,2} r_{g,15}^{-1}$ cm $^{-3}$, where $\alpha \sim 1$ is the dimensionless spin of the black hole and $r_{g,15} \equiv r_g / 10^{15}$ cm. For certain combinations of $\langle \epsilon \rangle$ and U_{ph} , the screening of the electric field can happen in the regime where the pair cascade is governed by the TPP process and Compton scattering in the deep Klein-Nishina regime (see e.g., black and blue curves in the left and right panels of Figure 4, respectively):

$$\langle \epsilon \rangle_0^2 U_{ph,0}^{-3/2} \gtrsim 0.02 M_9 B_{0,2}^{-1/2}, \quad (16)$$

where we used the condition $\lambda_{\max}^{-1} > t_E$, Equations (2),(14)-(15), and $M_9 \equiv M_{BH}/10^9 M_\odot$.

The characteristic timescale $t_* \equiv t_E = \lambda^{-1}$ can also be used to estimate the typical size of the gap as $h = ct_*$, which lies in the range $(0.01 - 1) r_g$ for all the cases displayed in Figure 4. The maximum electric field that can be developed in the gap dictates also the amount of dissipation in the magnetosphere. The gap power can be estimated as $P_{\text{gap}} \sim E_0 J A h$, where $A = \pi r_g^2$ is the cross sectional area of the jet funnel, and $J \sim Bc / (4\pi r_g)$ is the Goldreich-Julian current density required by the jet. As a comparison, the jet power is roughly $P_{\text{jet}} \sim \alpha B_0^2 A c / (64\pi)$, and one can write:

$$P_{\text{gap}} \sim \frac{16 E_0 h}{B_0 r_g} P_{\text{jet}}. \quad (17)$$

5.1. Application to M87

As an indicative example, we consider the radio galaxy M87 (NGC 4486) located at a distance $\simeq 16.7$ Mpc (Mei et al. 2007). Its soft photon spectrum peaks at 300 GHz, with a flux around 1 Jy (corresponding luminosity $L \sim 10^{42}$ erg s $^{-1}$), and an estimated photon index $\Gamma \sim 2.2$ above 300 GHz (see Broderick & Tchekhovskoy

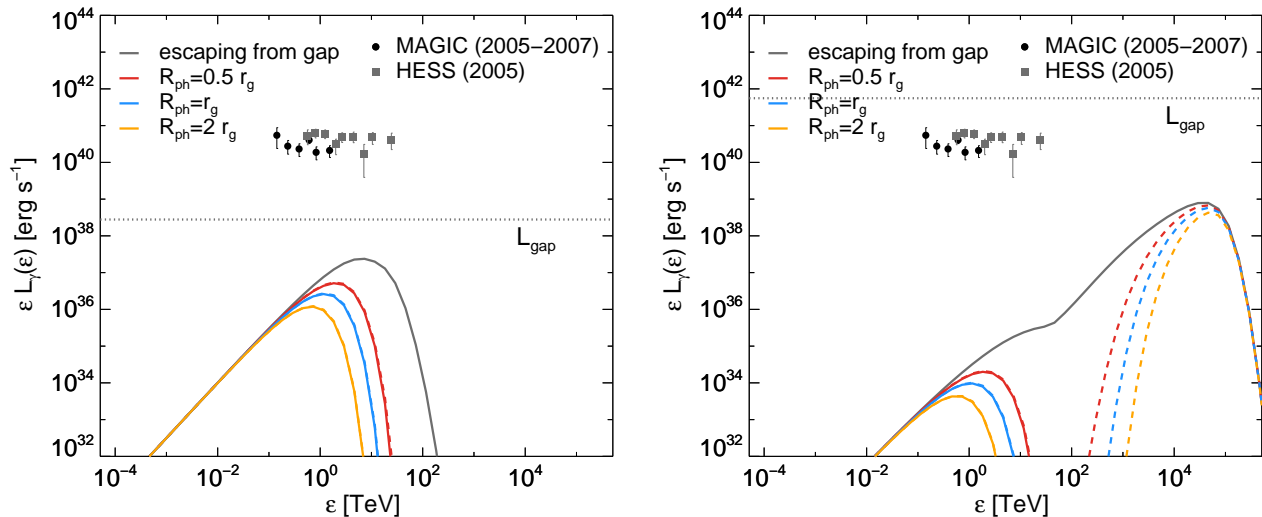


Figure 5. Photon energy spectra escaping from the gap (solid grey lines) for two indicative cases shown in the right panel of Figure 4 with parameters $E_0 = 5 \times 10^{-3}$ statV cm $^{-1}$, $h = 0.02 r_g$ (left panel) and $E_0 = 9 \times 10^{-1}$ statV cm $^{-1}$, $h = 0.2 r_g$ (right panel). Dashed colored lines show the attenuated gamma-ray spectra due to photon propagation in the ambient photon field, assuming different radii R_{ph} (see inset legends). Solid colored lines show the observed spectra after EBL attenuation for the M87 distance. Here, the model of Franceschini et al. (2008) was adopted. In both panels, the estimated gap power (see Equation (17)) is indicated by the horizontal dotted line. For comparison, we overplot two indicative spectra of M87 taken with MAGIC during a low state between 2005 and 2007 (Aleksić et al. 2012) and with H.E.S.S. during a flare in 2005 (Aharonian et al. 2006).

2015, and references therein). However, the actual amount of the soft radiation in the direct vicinity of the gap is quite uncertain. Following Chen et al. (2018), we adopt the 300 GHz frequency as the low-energy end of the power-law photon distribution, i.e., $\epsilon_{\min} = 1.2 \times 10^{-3}$ eV = $2.4 \times 10^{-9} m_e c^2$, and use $U_{ph} = L / (4\pi r^2 c) \sim 0.1$ erg cm $^{-3}$ as an estimate of the soft photon energy density at a distance $r \approx 3r_g$ from the black hole. The pair cascade growth rate for these parameters is shown by the red curve in the right panel of Fig. 4. The screening of the gap occurs in the low- E_0 (Thomson) regime (see crossover of the red and dashed grey lines) and the peak electric field is predicted to be $E_0 \sim 5 \times 10^{-3}$ statV cm $^{-1} \sim 5 \times 10^{-5} B_0$ for $B_0 = 100$ G, consistent with the estimation by Chen et al. (2018). In reality, the properties of the radiation field at the gap (e.g., U_{ph} and ϵ_{\min}) are highly uncertain. For example, if $\epsilon_{\min} \gtrsim 10^{-2}$ eV or $U_{ph} \lesssim 10^{-3}$ erg cm $^{-3}$, then the pair cascade would be regulated by triplet pair production and Klein-Nishina scatterings. Even though the mean free path for ICS scatterings in the Klein-Nishina regime is expected to be large, it is still possible to screen the electric field in the gap due to an extra source of pairs provided by the TPP process, an effect which has not been considered in the past for M87.

We next discuss the predictions of our gap model about the gamma-ray emission. To do so, we compute the escaping photon spectra for two indicative cases where the screening of the gap happens either in the low- E_0 regime (case A) or in the high- E_0 regime (case B). More specifically, we use the parameters that correspond to the intersection of the grey dashed line with the red-colored and blue-colored curves in the right panel of Figure 4. As discussed previously, the intersection of the curves provides an estimate of the gap size and power, which for cases A and B read respectively $h \sim 0.02 r_g$, $P_{\text{gap}} \simeq 3 \times 10^{38}$ erg s $^{-1}$ and $h \sim 0.2 r_g$, $P_{\text{gap}} \simeq 6 \times 10^{41}$ erg s $^{-1}$.

The photon spectra escaping from the gap for the two cases are presented in Figure 5 (solid grey lines). When the gap is screened in the low- E_0 regime (see left panel), the growth of the pair cascade takes place mostly in the Thomson regime, where pairs cool efficiently via ICS. As a result, the escaping gamma-ray luminosity is comparable to the gap power and the photon spectra typically extend from tens to hundreds of TeV depending on the parameters. For case A, in particular, we find $L_\gamma \approx P_{\text{gap}}/2$ and a peak photon energy of ~ 10 TeV (see left panel). On the contrary, if the gap is screened in the high- E_0 regime, where Klein-Nishina scatterings and TPP are important, the photon spectrum can ex-

tend to much higher energies (e.g., \gtrsim PeV), because electron cooling is suppressed (see right panel). This also means that a large fraction of the gap power that is being “pumped” into the pairs by the electric field is not radiated away. In this particular example, we find that $L_\gamma \sim 0.01 P_{\text{gap}}$. Thus, in both cases, the direct gamma-ray emission from the gap cannot explain the TeV observations of M87 (see symbols in Figure 5), but for different reasons: either the gap is screened in the Thomson regime and its power is low (left panel) or the gap is screened in the Klein-Nishina-TPP regime and its power is higher, but the radiative efficiency is low.

The gamma-ray spectrum that escapes from the gap is not necessarily the same as the observed one. Photons still have to propagate through the ambient radiation field, and the degree of the gamma-ray flux attenuation will depend on the typical size of the radiation R_{ph} , as illustrated in Figure 5 (see dashed colored lines in both panels). Gamma-ray photons with energy $\sim 3/\epsilon_{\text{min}}$ will have the shortest mean free path, and a large dip in the spectrum is expected at this energy, as shown in the right panel of the figure. Photons with either much lower or higher energy will suffer less attenuation.

The absorbed gamma-rays will initiate a post-gap pair cascade, and the absorbed luminosity will re-emerge at lower energies with a spectrum that will depend on the interplay of various cooling processes (e.g., curvature, synchrotron, ICS in the Thomson or Klein-Nishina regimes). Although the attenuated luminosity, for both cases considered here, will be a small fraction of the observed TeV luminosity of M87, the outflowing pairs from the gap will still carry most of the gap power in case B. Thus, if these ultra-relativistic pairs are able to lose their energy in the post-gap region via channels other than ICS and TPP (e.g., curvature radiation), a radiative signal with $L_\gamma \sim P_{\text{gap}}$ is expected. A detailed study of the post-gap cascade emission will be presented elsewhere.

6. DISCUSSION

We have presented numerical calculations of pair-Compton cascades in the Thomson and Klein-Nishina regimes and investigated the effects of triplet pair production. By adopting a simplified model for the acceleration region and using the method of transport equations for the particle evolution, we computed the growth rate of the pair cascade as a function of the accelerating electric field in the presence of black-body and power-law ambient photon fields. Informed by our numerical results, we derived simple analytical scalings of the growth rate (see Eqs. 13 and 14) and the corresponding electric field (Eq. 2) on the properties of the background

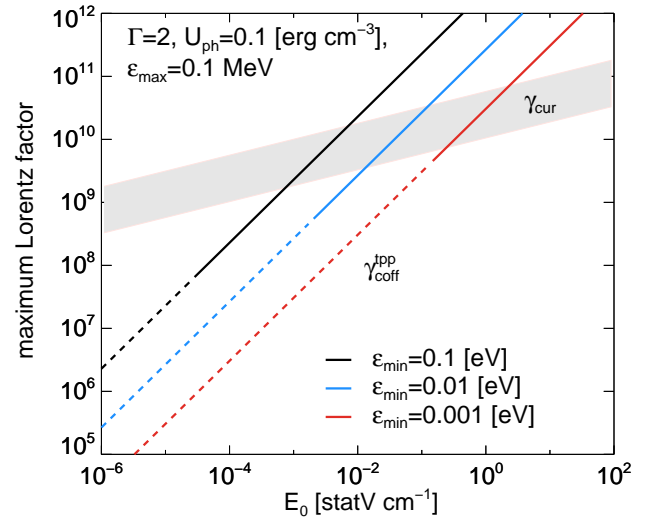


Figure 6. Limiting Lorentz factor due to energy losses by curvature radiation (see Equation (18)) as a function of the electric field, for curvature radii ranging from 1 to $30 r_g$ of a black hole with mass $M_{\text{BH}} = 6.5 \times 10^9 M_\odot$ (grey-colored band). Solid colored lines show an estimate for the cutoff Lorentz factor of the pair distribution (see Equation (19)) in the regime where TPP dominates the production of pairs, for different values of the minimum energy of the ambient power-law photon field (see inset legend; same as in the right panel of Figure 4). The expression given by Equation (19) is not valid in the low- E_0 regime (dashed lines). A colored version of this plot is available online.

photon field. For certain parameters, which can be realized in the vicinity of AGN black holes, the pair cascade may well be regulated by triplet pair production and Compton scatterings in the deep Klein-Nishina regime.

Even if the physical conditions in the acceleration region (i.e., background photon field and electric field strength) are such as to ensure the development of the pair cascade in the deep Klein-Nishina regime, this may not be realized if pairs can lose energy via a process other than TPP and ICS. Because of the ultra-relativistic energies involved in the high- E_0 regime (see right panel in Figure 1), the most relevant energy loss process becomes curvature radiation. The limiting Lorentz factor in this case is:

$$\gamma_{\text{cur}} \simeq 10^{10} E_{0,2}^{1/4} M_9^{1/4} \left(\frac{\rho_c}{r_g} \right)^{1/2} \quad (18)$$

where ρ_c is the typical radius of curvature for a particle trajectory, which is assumed to be independent of the particle energy. In the high- E_0 (TPP-dominated) regime (i.e., for $E_0 \gtrsim E_0^{(\text{KN})} \simeq 5 \times 10^{-4} U_{ph,0} \langle \epsilon \rangle_0^{-2}$ statV

cm^{-1}), the cutoff Lorentz factor of pairs can be approximated by⁵:

$$\begin{aligned}\gamma_{\text{coff}}^{(tpp)} &\approx 2 \times 10^{13} E_{0,2} \frac{\epsilon_{\text{min},-1}}{U_{ph,0}} \ln \left(\frac{\epsilon_{\text{max},5}}{\epsilon_{\text{min},-1}} \right) \\ &\approx 1.4 \times 10^{13} E_{0,2} \langle \epsilon \rangle_0 U_{ph,0}^{-1}\end{aligned}\quad (19)$$

where the notation $\epsilon_{j,x} = \epsilon_{j,x}/(10^x \text{ eV})$ was introduced, a power-law photon field with $\Gamma = 2$ and $\epsilon_{\text{max}} \gg \epsilon_{\text{min}}$ was assumed, and Equation (6) was used to derive the second expression. Curvature losses can be neglected as long as $\gamma_{\text{coff}}^{(tpp)} \lesssim \gamma_{\text{cur}}$ or equivalently:

$$\langle \epsilon \rangle_0 U_{ph,0}^{-1} \lesssim 7 \times 10^{-4} E_{0,2}^{-3/4} M_9^{1/4} \left(\frac{\rho_c}{r_g} \right)^{1/2}. \quad (20)$$

Figure 6 shows the two characteristic Lorentz factors as a function of E_0 for different values of the minimum energy ϵ_{min} of a power-law photon field with index 2. If, for a given E_0 , $\gamma_{\text{coff}}^{(tpp)} > \gamma_{\text{cur}}$, then the actual growth rate of the pair cascade will be lower than the one obtained in Section 4. For the indicative parameters of the photon field in M87 that we adopted in the previous section (i.e., $U_{ph} = 0.1 \text{ erg cm}^{-3}$ and $\epsilon_{\text{min}} = 10^{-3} \text{ eV}$) we find that $\gamma_{\text{coff}}^{(tpp)}$ becomes comparable to γ_{cur} only for $E_0 \sim 0.1 - 1 \text{ statV cm}^{-1}$ (see red line in Figure 6). However, our simplified model predicts that the electric field will not be able to grow to such values and that the gap will be screened by the pair growth in the Thomson regime, as shown in Figure 4 (see red curve in right panel). Nevertheless, for other photon field parameters the pair cascade may develop in the TPP-dominated regime before the particle energy is limited by curvature losses (see e.g., black and blue lines in Figure 6).

In this work, we studied the pair cascade under the assumption of a time-independent electric field. This is a good approximation, if the particle acceleration timescale is much shorter than the timescale for the electric field to evolve. In a dynamic gap, if the electric field grows quadratically with time, as in Equation (15), the condition $t_{\text{acc}}(\gamma_{eq}) < t_E$ in the low- E_0 regime can be written as:

$$\frac{E_0}{B_0} > \left(\frac{3}{8\pi} \right)^{1/2} \left(\frac{r_B}{r_g} \right)^{1/2} \left(\frac{\ell_{\text{IC}}^{\text{tot}}}{r_g} \right)^{1/2} \left(\frac{m_e c^2}{\langle \epsilon \rangle} \right)^{1/2}, \quad (21)$$

where we used Equation (1), $r_B = m_e c^2 / (q_e B_0) \approx 17 B_{0,2}^{-1} \text{ cm}$ and $\ell_{\text{IC}}^{\text{tot}} = \langle \epsilon \rangle / \sigma_T U_{ph}$ is the mean free path for IC scattering on the overall soft photon energy distribution. For U_{ph} and B_0 values typical for

the black-hole environment of AGN, Equation (21) becomes $E_0/B_0 > 10^{-5} M_9^{-1} B_{0,2}^{-1/2} U_{ph,0}^{-1/2}$, and can be easily satisfied. In the high- E_0 (TPP-dominated) regime, the condition on the timescales reads $t_{\text{acc}}(\gamma_{\text{coff}}^{(tpp)}) < t_E$ or equivalently:

$$\frac{E_0}{B_0} \gtrsim 0.01 M_9^{-1} U_{ph,0}^{-2} \langle \epsilon \rangle_0^2, \quad (22)$$

where we used Equation (19) and considered a power-law soft photon field with $\Gamma = 2$. This condition is more restrictive than the one in Equation (21), since the pairs in the TPP-dominated regime reach ultra-relativistic energies and thereby have much longer acceleration timescales. It is therefore possible that the assumption of constant electric field breaks down in the high- E_0 regime for certain parameters. In the case where the acceleration time is no more negligible, the growth of the electric field and its response to pair creation should be taken into account. Moreover, our simplifying assumption of identical particles, which disregards the deceleration of positrons, is questionable. In order to simulate the cascade in this case, a proper particle-in-cell (PIC) treatment (Levinson & Cerutti 2018; Chen et al. 2018) with inclusion of both ICS and TPP processes is necessary. This will be carried out in a dedicated future work.

Here, we have studied the development of pair cascades initiated by $\gamma\gamma$ absorption of γ -ray photons produced by accelerated electrons in a gap. It is also possible that a non-relativistic proton enters the charge-starved region and accelerates to high energies (Bednarek & Protheroe 1999). In this case, one expects that protons will start producing pairs via the Bethe-Heitler process ($p\gamma \rightarrow pe^-e^+$) on ambient soft photons with energy ϵ_0 when they reach a Lorentz factor $\gamma_p^{(pe)} \gtrsim 2m_e c^2 / \epsilon_0$. The pairs will be injected into the gap with relativistic Lorentz factors and a broad energy spectrum (Mastichiadis et al. 2005; Kelner & Aharonian 2008; Petropoulou & Mastichiadis 2015). Similar to the pairs produced by $\gamma\gamma$ pair production, the Bethe-Heitler pairs can initiate electromagnetic cascades leading to high multiplicities (i.e., large number of secondary pairs per proton). It is therefore likely that the electric field will be screened before the protons reach the required energy to produce pions and, in turn, neutrinos, as the threshold for photo-meson production ($p\gamma \rightarrow n\pi^+(p\pi^0)$) is higher, namely $\gamma_p^{(p\pi)} \gtrsim m_\pi c^2 / \epsilon_0$, where m_π is the pion mass. However, if the background photon field has a wide energy spectrum (e.g., power law), then even lower energy protons can interact with sufficiently high-energy photons to produce neutrinos. The computation of the escaping neutrino and γ -ray

⁵ The logarithmic dependence of the TPP cross section is neglected when deriving this expression.

fluxes in this scenario, which becomes relevant in light of the recent neutrino detections from the γ -ray AGN TXS 0506+056 (IceCube Collaboration et al. 2018a,b), requires a dedicated study of the ensued pair cascade.

The authors thank the anonymous referee for useful suggestions that helped to improve the manuscript. This research was motivated by discussions at the 2018

MIAPP workshop “The High Energy Universe: Gamma Ray, Neutrino, and Cosmic Ray Astronomy”. It is supported by the Munich Institute for Astro- and Particle Physics (MIAPP) of the DFG cluster of excellence “Origin and Structure of the Universe”. M.P. and Y.Y. acknowledge support from the Lyman Spitzer, Jr. Postdoctoral Fellowship. MP acknowledges support also from the Fermi Guest Investigation grant 80NSSC18K1745. A.C. acknowledges support from NASA grant NNX15AM30G.

REFERENCES

- Aharonian, F., Akhperjanian, A. G., Bazer-Bachi, A. R., et al. 2006, *Science*, 314, 1424
- Akharonian, F. A., Kririllov-Ugrumov, V. G., & Vardanian, V. V. 1985, *Ap&SS*, 115, 201
- Aleksić, J., Alvarez, E. A., Antonelli, L. A., et al. 2012, *A&A*, 544, A96
- Anguelov, V., Petrov, S., Gurdev, L., & Kourtev, J. 1999, *Journal of Physics G Nuclear Physics*, 25, 1733
- Bednarek, W., & Kirk, J. G. 1995, *A&A*, 294, 366
- Bednarek, W., & Protheroe, R. J. 1999, *MNRAS*, 302, 373
- Beskin, V. S., Istomin, Y. N., & Pev, V. I. 1992, *Soviet Ast.*, 36, 642
- Blandford, R. D., & Znajek, R. L. 1977, *MNRAS*, 179, 433
- Blumenthal, G. R., & Gould, R. J. 1970, *Reviews of Modern Physics*, 42, 237
- Broderick, A. E., & Tchekhovskoy, A. 2015, *ApJ*, 809, 97
- Chen, A. Y., Yuan, Y., & Yang, H. 2018, *ApJ*, 863, L31
- Coppi, P. S., & Aharonian, F. A. 1997, *ApJ*, 487, L9
- Event Horizon Telescope Collaboration, Akiyama, K., Alberdi, A., et al. 2019, *ApJ*, 875, L1
- Franceschini, A., Rodighiero, G., & Vaccari, M. 2008, *A&A*, 487, 837
- Gould, R. J., & Rephaeli, Y. 1978, *ApJ*, 225, 318
- Gould, R. J., & Schröder, G. P. 1967, *Physical Review*, 155, 1404
- Haug, E. 1981, *Zeitschrift Naturforschung Teil A*, 36, 413
- Hirovani, K., & Okamoto, I. 1998, *ApJ*, 497, 563
- Hirovani, K., & Pu, H.-Y. 2016, *ApJ*
- IceCube Collaboration, Aartsen, M. G., Ackermann, M., et al. 2018a, *Science*, 361, eaat1378
- . 2018b, *Science*, 361, 147
- Katsoulakos, G., & Rieger, F. M. 2018, *ApJ*, 852, 112
- Kelner, S. R., & Aharonian, F. A. 2008, *PhRvD*, 78, 034013
- Lee, S. 1998, *PhRvD*, 58, 043004
- Levinson, A., & Cerutti, B. 2018, *A&A*, 616, A184
- Levinson, A., & Rieger, F. 2011, *ApJ*, 730, 123
- Mastichiadis, A. 1986, *A&A*, 169, 373
- . 1991, *MNRAS*, 253, 235
- Mastichiadis, A., & Kirk, J. G. 1995, *A&A*, 295, 613
- Mastichiadis, A., Marscher, A. P., & Brecher, K. 1986, *ApJ*, 300, 178
- Mastichiadis, A., Protheroe, R. J., & Kirk, J. G. 2005, *A&A*, 433, 765
- Mei, S., Blakeslee, J. P., Côté, P., et al. 2007, *ApJ*, 655, 144
- Petrovou, M., & Mastichiadis, A. 2015, *MNRAS*, 447, 36
- Protheroe, R. J. 1986, *MNRAS*, 221, 769
- Protheroe, R. J., Mastichiadis, A., & Dermer, C. D. 1992, *Astroparticle Physics*, 1, 113
- Ruderman, M. A., & Sutherland, P. G. 1975, *ApJ*, 196, 51
- Settimo, M., & De Domenico, M. 2015, *Astroparticle Physics*, 62, 92
- Timokhin, A. N., & Arons, J. 2013, *MNRAS*, 429, 20
- Timokhin, A. N., & Harding, A. K. 2019, *ApJ*, 871, 12
- Wang, K., Liu, R.-Y., Li, Z., & Dai, Z.-G. 2017, *PhRvD*, 95, 063010
- Zdziarski, A. A. 1988, *ApJ*, 335, 786
- Zdziarski, A. A., Malzac, J., & Bednarek, W. 2009, *MNRAS*, 394, L41